Atomic Layer Deposition of Boron-Containing Layers Using a Combined Trimethylborate- and Water-based Plasma

Arpan Dhara[1], Andreas Werbrouck[1], Jin Li[1], Tippi Verhelle[1], Matthias Minjauw[1], Johan Meersschaut[2], Lowie Henderick[1], Jolien Dendooven[1], Christophe Detavernier[1,]*

[1]Department of Solid State Sciences, CoCooN research group, Krijgslaan 281 S1, 9000 Ghent University, Belgium

[2]imec, Kapeldreef 75, B-3001 Heverlee, Belgium

* Corresponding author: christophe.detavernier@ugent.be

ABSTRACT

Trimethyl borate (TMB), a commonly used boron precursor for depositing boron-containing thin films via atomic layer deposition (ALD), poses several limitations, including low boron incorporation, growth inhibition, and process temperature constraints. Despite TMB's high vapor pressure and thermal stability, its limited reactivity leads to slow and incomplete surface reactions in thermal processes. Plasma-enhanced processes employing oxygen plasma as reactant, although effective in avoiding carbon impurities, tend to produce films with low boron content. To overcome these limitations, we initially explored the use of TMB plasma as a reactant, inspired by the success of trimethyl phosphate (TMP) plasma in the synthesis of various ALD metal phosphates. However, TMB alone in plasma form proved ineffective as a reactant due to the absence of a temperature window for self-limiting growth on the substrate surface. In response, we developed an approach that combines TMB with H_2O as a co-reactant in the plasma phase. This method demonstrated self-limiting growth at and above 250°C, a significantly higher growth per cycle (~3.5 Å), and a marked increase in boron concentration (>25% increase vs O_2 plasma process and >85% increase vs thermal process) in the aluminum borate thin films. The underlying growth mechanisms were analyzed using *in situ* ellipsometry, *in vacuo* X-ray photoelectron spectroscopy (XPS), and time-resolved quadruple mass spectrometry (QMS). These findings not only provide valuable insights into the deposition of aluminum borate films but also provide a promising pathway for the development of other metal borates or boron-containing layers by the ALD technique.

INTRODUCTION

Metal borates or boron containing thin films have emerged as promising materials in various applications, including micro-electronics,[1,2] neutron detection,[3,4] electrocatalysis,[5,6] energy storage[7,8] and biomedical coatings[9]. For example, zinc borate thin films have been studied as dielectric layers for field-effect transistors;[10] alkali metal borate,[11] borophosphate[12,13] and borocarbonate[14,15] thin films have been considered as electrolytes for solid-state thin film batteries. For biomedical applications, borate glasses offer better bioactivity and healing capability compared to silicate and phosphate analogues.[9] Zhang et al showed how 1-10% boron incorporation in In_2O_3 and Al_2O_3 layers can improve the metal oxide thin film transistor performance.[16] Results indicate that boron doping suppress the defects related to electron traps and carrier generation in In_2O_3 channel layer. On the other hand, boron incorporation in Al_2O_3 layer improves the dielectric constant, refractive index and leakage current.

The most fundamental boron-containing layer, B_2O_3, has high hygroscopicity and forms volatile boric acid (H_3BO_3), making it challenging to handle.[2] As a result, researchers have explored ternary oxides and B-doped oxides as alternatives using several deposition techniques. Because of its self-limiting nature and unparalleled conformality over complex structures, atomic layer deposition (ALD) has been used as preferred method for depositing thin films compared to many other techniques.[17] Depositing ternary materials by ALD has been mostly achieved using an ALD 'supercycle' approach.[18] In the case of boron-containing layers, supercycles consist of metal oxide and boron oxide sub-cycles, where in principle the ratio between the two defines the film composition. However, achieving the desired boron concentration in these films has been a persistent challenge. When the metal oxide to boron oxide cycle ratio is 1:1, the boron concentration is usually low, ranging from 1-10%. In principle, a further increase in boron

concentration could be achieved by increasing the number of B_2O_3 sub-cycles, however B_2O_3 ALD shows growth inhibition and needs reactivation of the surface after a few cycles.[18]

The unavailability of suitable precursors is one of the major issues in producing borate layers by ALD. A comprehensive overview of boron precursors employed in ALD processes can be found in our previous publication.[19] Typically, boron alkoxides like trimethyl borate (TMB) have been favored due to their high volatility, thermal stability, and cost effectiveness. However, limited reactivity poses a hindrance to their efficacy as ALD precursor. In a noteworthy development, Saly et al. introduced metal tris(pyrazolyl)borate as a novel class of ALD precursors to obtain stoichiometric borate films.[20,21] Nevertheless, their high vaporization temperature (~200 °C) imposes practical limitations.

To overcome these challenges, the quest for an ideal precursor and a convenient process becomes imperative. One might consider boric acid (H_3BO_3) as an ideal boron source for ALD, however boric acid exhibits a gradual release of water and forms metaboric acid when subjected to heat ($H_3BO_3 \rightarrow HBO_2 + H_2O$).[22,23] In pursuit of this, Mane et al. explored various strategies to grow boron-comprising aluminum oxide layers, employing trimethyl aluminum (TMA) with boric acid, boric acid dissolved in methanol, and TMB in different combinations of pulse sequences.[24] Surprisingly, no boron was detected in the films obtained from the combination of TMA, boric acid and water (TMA-H_3BO_3-H_2O). This suggests a lack of interaction between TMA and boric acid molecules. Conversely, when boric acid was mixed with methanol and used as a precursor, the resulting films contained 8-12% boron with carbon impurity. It is speculated in this case that the solution undergoes a transformation, generating water and TMB *in situ* ($H_3BO_3 + 3CH_3OH \rightarrow B(OCH_3)_3 + 3H_2O$). Consequently, water molecules initially interact with surface ─$Al(CH)_3$ to form ─Al(OH) surface groups, followed by interactions with TMB molecules. Mattelaer et al.

achieved localized boron and hydrogen incorporation within aluminum oxide films by using TMB and oxygen plasma.[19] These as-grown films, configured in a 1:1 supercycle, were found to contain approximately 5% boron and roughly 15% hydrogen.

Similar struggle could be found for ALD of metal phosphates. Most of the ALD processes related to metal phosphates result in poor phosphorus uptake. Our group came up with a novel concept of plasma polymerization of trimethyl phosphate (TMP) and used plasma-activated TMP molecules as a precursor to grow several metal phosphates.[25–30] In this way, it was possible to obtain metal phosphate ALD with a higher growth rate (~1 nm per cycle) and significantly larger phosphorus content. Owing to the success of that concept, it was intriguing to explore TMB plasma in the same manner to grow metal borate thin films. Previously, TMB plasma has been employed in chemical vapor deposition (CVD) processes to grow boron oxide or boron-doped diamond thin films. It has been often combined with co-reactant gases like O_2, N_2, H_2, and CO_2 together with TMB in order to change reaction kinetics, resulting in a different percentage of boron incorporation into the films.[31,32] Employing a similar approach during an ALD process could be an effective strategy to produce complex borate materials in conjunction with a significantly higher growth rate.

In this study, we explored a unique 'combined plasma' ALD approach, to produce high-quality aluminum borate thin films using TMB as the common boron source. The new process is compared to conventional thermal ALD processes, using TMA, TMB and H_2O, and to plasma-enhanced ALD processes using TMA, TMB and oxygen plasma. While the thermal processes exhibit moderate growth per cycle and carbon impurities, the plasma-enhanced process with two oxygen plasma steps shows impurity-free layers but still suffers from a low boron concentration. Remarkably, by introducing a combination of TMB and H_2O in plasma form, we achieved self-

limiting growth with significantly higher growth rates and a larger amount of boron incorporation in the aluminum borate films. We attribute this to *in situ* polymerization of TMB and termination of this process by hydrolysis of the surface groups with OH radicals in the plasma. To elucidate the underlying mechanisms, we conducted *in vacuo* X-ray photoelectron spectroscopy (XPS) and *in situ* transient quadruple mass spectrometry (QMS) studies.

EXPERIMENTAL PROCEDURES

All ALD films have been deposited in a custom-built pump-type ALD reactor with a base pressure of 1×10^{-6} mbar. The reactor walls were heated to 100 °C to prevent precursor condensation. To deposit aluminum borate films, we used a combination of trimethyl aluminum (TMA), trimethyl borate (TMB) and H_2O. TMA and TMB, obtained from Sigma-Aldrich, as well as the deionized H_2O, were kept at room temperature.

We have explored four different types of ALD processes: (1) a *thermal process*, where one ALD cycle involved an exposure sequence of TMA – H_2O – TMB – H_2O, (2) an *O_2-plasma process*, where one ALD cycle involved an exposure sequence of TMA – O_2 plasma – TMB – O_2 plasma, (3) a *TMB-plasma approach* which unfortunately did not prove self-limiting, and (4) a *'combined plasma' process*, where one ALD cycle involved an exposure sequence of TMA – (TMB+H_2O) plasma – H_2O plasma. Key results for the thermal and O_2-plasma based processes are described in the main text with most graphs added as Supplementary Information, while results and data for the TMB-plasma and combined plasma approaches are included in the main text.

During the thermal process, the precursor partial pressure was maintained at 5×10^{-3} mbar, with a 30 second pump time after each precursor dose. For the oxygen plasma process, the plasma pressure was maintained at 10^{-2} mbar. In the combined-plasma process, the partial pressures were $\leq10^{-4}$ mbar for TMB, and 5×10^{-3} mbar for H_2O.

The elemental composition of the thin films was determined with time-of-flight energy elastic recoil detection analysis (ERD). For this analysis, we deposited approximately 50 nm thick films on TiN coated Silicon substrate. TiN coated substrate was used to have a better interface contrast in the data. The data were obtained with an 8.010 MeV ^{35}Cl ion beam impinging on the sample at a glancing angle of 20°. The telescope containing the time-of-flight and energy detectors was at a scattering angle of 40°. The sample was moved during the data acquisition to minimize the effect of beam-induced hydrogen desorption. In the coincidence spectra of time-of-flight and energy the recoil signals from H, ^{10}B, ^{11}B, C, O are well discriminated from the signals from Ti and N in the sample. The intensities of the various detected ions as a function of time-of-flight were transformed to concentration depth profiles with an iterative procedure. The analysis considered the detection efficiency of the telescope for H ions. The concentration of the element boron was derived from the ^{11}B signal, corrected for the natural isotope abundance. The reported uncertainties have a confidence level of 95%. The model to estimate the uncertainties was based on the statistical study of the repeatability and on the study of reference samples which were qualified with Rutherford backscattering spectrometry. The ERD analysis at imec has an ISO 9001 certification.

In situ ellipsometry using a J. A. Woollam model M-2000 ellipsometer with a wavelength range of 245–1000 nm was employed for growth studies. The measured data were fitted using a Cauchy model in the CompleteEase software package to obtain the film thickness. Elemental compositions were determined using a Thermo Scientific Theta Probe X-ray photoelectron spectroscopy (XPS) system with a monochromatic Al Kα excitation source (15 kV, 70 W) focused into a 300 µm spot on the surface and under an incidence angle of 30° with respect to the surface normal. The input lens of the concentric hemispherical analyzer is at an angle of 50° (take-off angle) with respect to the surface normal and an azimuthal angle of 110° with respect to the X-ray monochromator, and

accepts electrons over a wide angular range (20°-80° with respect to the surface normal). XPS depth profiling was performed by etching the samples with argon ions (3 kV, 2 μA) in an area of 2 mm x 2 mm on the sample surface under an incidence angle of 45° with respect to the surface normal. *In vacuo XPS* experiments were carried out using a custom-built system that connects the ALD chamber to the Thermo Scientific Theta Probe system. The silicon substrates were heated, exposed to the precursors in the ALD chamber, transferred back to the XPS chamber, and measured without exposure to air. This approach provides valuable insights into the reaction pathways and chemistry in the ALD process. Survey scans were acquired at 200 eV pass energy with a 0.5 eV step size, detail scans were acquired at 100 eV pass energy with a step size of 0.1 eV. XPS data analysis was performed using the CasaXPS software package.[33] The data were calibrated by setting the Si component in the Si 2p spectrum at 99.4 eV.

Optical emission spectra (OES) of different plasma species were measured using an Ocean Optic QE Pro spectrometer coupled with an optical fiber to the plasma column and analyzed with SpectralSuite software.

For *in situ QMS* analyses, we employed a Hiden HPR-30 mass spectrometer with secondary electron multiplier (SEM) detector. This technique offers insights into precursor delivery and depletion and detection of reaction byproducts and intermediates. By acquiring full-range spectra (for example, m/z=1-200 amu (atomic mass unit)) through an innovative cyclic ALD process manipulation,[34,35] we were able to study transient measurements and gain a comprehensive understanding of the reaction mechanism. The combination of *in vacuo* XPS and *in situ* mass spectrometry allowed us to explore the underlying mechanisms of the various ALD routes that were explored towards depositing aluminum borate.

RESULTS

Exploring a TMB-plasma-based approach. The plasma-induced polymerization of monomer molecules leading to the formation of highly disordered crosslinked networks is a well-known phenomenon.[36] It has been observed that at low temperature, the polymerized species can grow on a substrate surface. In a pioneering study by Dobbelaere et al., it was demonstrated that trimethyl phosphate (TMP) undergoes polymerization in the plasma and can be deposited on a substrate at low temperatures.[25] However, as the substrate temperature increases, the thermodynamics of the plasma polymerization process become unfavorable for sustaining continuous growth, instead entering a regime where self-limiting growth characteristics can be achieved, making it a suitable exposure step during an ALD processes. The successful deposition of various metal phosphates using TMP plasma has been reported, as listed in a recent review paper.[37]

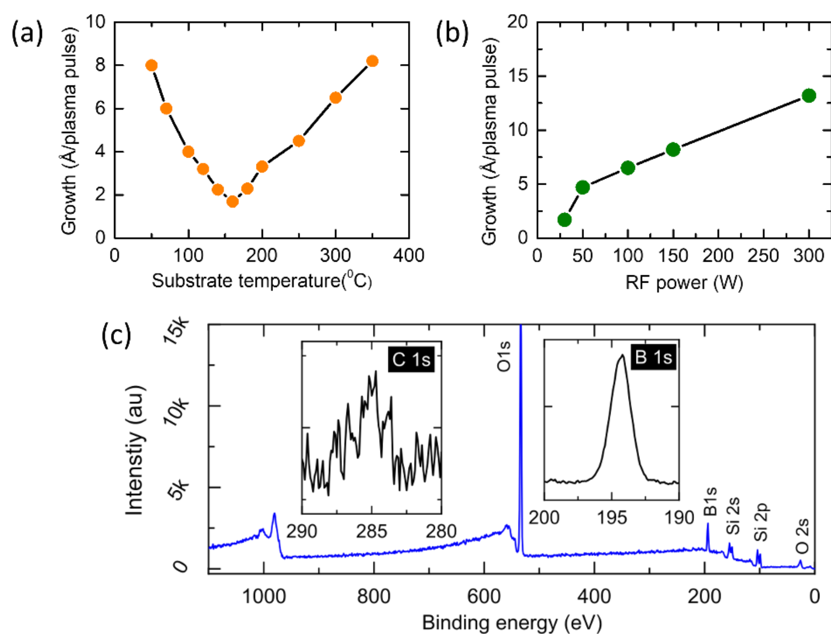

Figure 1: Characteristics of TMB plasma polymerization. (a) growth *vs.* substrate temperature for a 10 second 1×10^{-3} mbar TMB plasma pulse at 100-watt RF power, (b) growth *vs.* RF power for a 10 second 1×10^{-3} mbar TMB plasma pulse at 300°C substrate temperature, and (c) XPS

survey and high-resolution boron and carbon 1s spectra of an as-deposited layer obtained from a 20 second TMB plasma pulse at 300 °C substrate temperature, measured without exposing the sample to air.

Building upon the success of TMP plasma, we sought to explore whether metal borates could be grown using a similar approach, employing TMB in plasma form. Therefore, *in situ* ellipsometry was used to monitor the growth on a Si substrate when sequentially pulsing TMB plasma into the reactor (without pulsing another reactant in between). This was done for a range of substrate temperatures and RF power settings. For each condition, the growth per plasma pulse was extracted from the linear slope of the *in situ* growth curve and plotted in Figure 1. Figure 1a displays the growth obtained from a 10 second TMB plasma exposure at different substrate temperatures and with a TMB pressure of 1×10^{-3} mbar. The growth rate decreases with increasing substrate temperature until approximately 150 °C, after which it gradually increases.

Plasma polymerization is a highly spontaneous process, but to achieve self-limiting growth suitable for ALD, certain conditions must be met to inhibit continuous (CVD type) deposition. This inhibition of continuous deposition typically occurs at elevated substrate temperatures, where spontaneous growth is suppressed—commonly referred to as the ceiling point (T_c).[25]

In the previous work using trimethyl phosphate (TMP) as a precursor for plasma polymerization, we successfully deposited ALD-grown metal phosphate films, with a critical temperature of ≥300 °C. However, in the case of TMB plasma polymerization, this critical point was not reached within the investigated temperature range of 35–350 °C. Initially, the observed decrease in growth rate can be attributed to the increasing influence of the TΔS term in the Gibbs free energy equation ($\Delta G = \Delta H - T\Delta S$). As the temperature increases, the entropy term ($T\Delta S$) grows larger, making ΔG towards positive value. However, beyond approximately 150 °C, we hypothesize that the reaction

follows an alternative pathway. We believe the subsequent increase in growth rate is related to a multistep dehydration or decomposition process.

Boric acid is known to undergo a multistep decomposition process ($H_3BO_3 \rightarrow HBO_2 \rightarrow B_2O_3$), with the first transition typically occurring around 100 °C and the second at approximately 160 °C.[23,22] In our case, we hypothesize that the observed change in growth rate is somehow related to this second transition. At temperatures above 150 °C, the surface species formed on the substrate during the plasma step readily react with incoming plasma species and undergo rapid de-hydroxylation, leading to the formation of oxide-like material. Figure 1b demonstrates that the degree of polymerization exhibits a linear relationship with RF power. Notably, when an as-deposited film obtained from TMB plasma (300 °C) was characterized using XPS without exposure to air (as shown in Figure 1c), the analysis revealed the presence of boron and oxygen along with a small amount of carbon, ranging from 1-2 atomic percentage, in the film. So, in principle TMB plasma can be used to grow high quality boron oxide films in CVD manner. As-grown films obtained from TMB plasma found to be amorphous in nature. This type of layer could be interesting for applications like boron doping and surface modification.[1,2,13]

Self-limiting growth for a (TMB+H_2O) combined plasma. To achieve self-limiting growth during plasma polymerization of TMB, we explored an alternative approach. Since B_2O_3 films are known to be hygroscopic and form boric acid in the presence of water ($B_2O_3 + 3H_2O \rightarrow 2H_3BO_3$),[2] we presumed that combining water with TMB in plasma could result in the formation of highly hydroxylated and less interlinked intermediate species, thereby inhibiting continuous growth on the substrate. Figure 2a indicates that complete inhibition, or the 'ceiling point', was attainable at substrate temperatures above 250 °C. After optimizing the process, we identified a suitable combination of partial pressures, namely ~5×10^{-3} mbar for H_2O vapor and $\leq1\times10^{-4}$ mbar for TMB

vapor, to attain this growth inhibition. Unless otherwise specified, these partial pressures were utilized for all investigations in this study. Notably, when the TMB pressure increased to 1×10^{-3} mbar the growth was no longer quenched, but instead a growth rate of ~0.2 Å was observed. We hypothesize that hydroxyl ions or radicals generated from water in the plasma play a key role in terminating the polymerization process, resulting in the formation of a (mono)layer of hydroxylated boron-containing species on the substrate. A similar inhibition of the growth was also observed when oxygen was used as mixing gas in the plasma, albeit to a lesser extent compared to water (Figure 2b), as the presence of OH radicals in the plasma is lower with oxygen compared to water. In contrast, as also presented in Figure 2b, the growth rate was significantly higher with argon as mixing gas due to the absence of OH radicals in the plasma. Optical emission spectra (OES) of the different plasma combinations shown in Figure 2c clearly demonstrate the difference. The main notable feature is the strong OH emission line near 320 nm in the case of H_2O as the mixing gas with TMB, which strongly decreases in intensity for O_2 in the plasma mix and is nearly absent when Ar is used. These findings suggest that the presence of OH radicals in the plasma is crucial for achieving self-limiting growth, making this (TMB+H_2O) plasma approach viable for ALD processes.

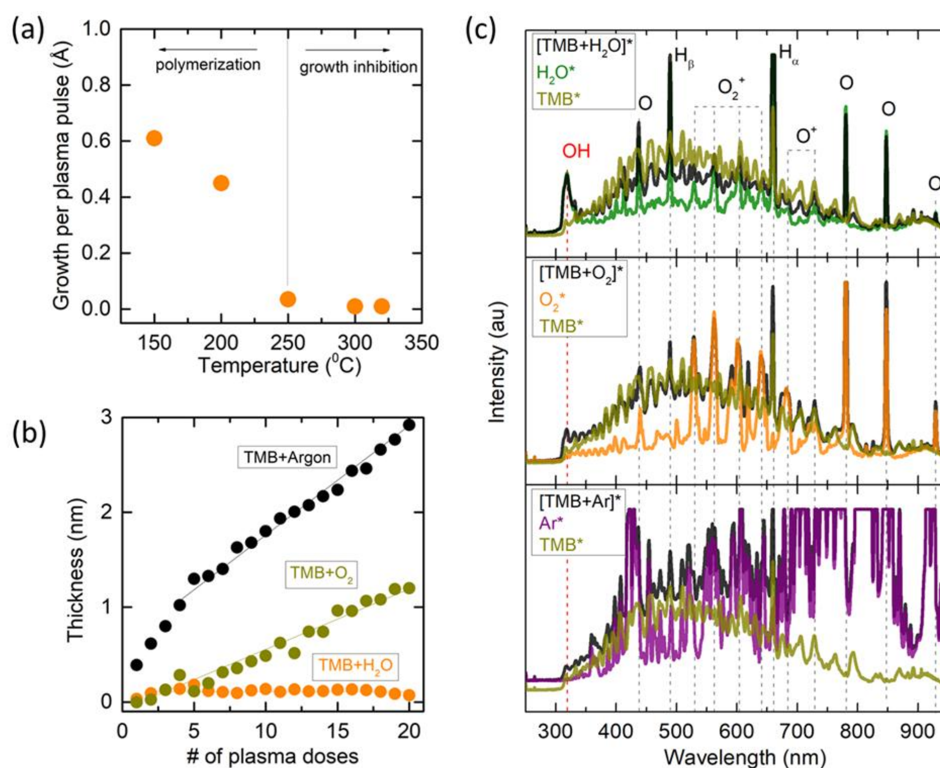

Figure 2: (a) Temperature dependent growth rate for a 10 sec (TMB+H_2O) plasma pulse, (b) growth characteristics of different combinations of gases with TMB in plasma at a temperature of 300 °C, and (c) optical emission spectra (OES) of different combinations of plasma.

Aluminum borate ALD using (TMB+H_2O) combined plasma approach. Following the achievement of self-limiting condition, we attempted to grow aluminum borate films using TMA and TMB plasma with water as mixing gas. Saturation conditions were determined based on the length of the plasma exposure while the TMA pulse was held at 10 seconds, and the deposition temperature was set at 300 °C. Figure 3a demonstrates that a saturated growth of ~3.4 Å per cycle can be achieved with a pulse time of 20 seconds or longer. It should be noted that an additional 10 second water plasma step was applied in absence of TMB. This additional step effectively removes carbon contamination and is discussed in detail in the *in vacuo* XPS and *in situ* QMS sections below. Similarly, the saturation of the TMA pulse was studied while keeping the plasma exposure

time constant at 20 seconds. It was found that a 5 second TMA pulse time was sufficient to achieve saturation. For all subsequent studies, we adopted the standard saturated conditions of 5 seconds for TMA and 20 seconds for the combined plasma pulses along with 10 seconds extra water plasma time (with a pumping step in between).

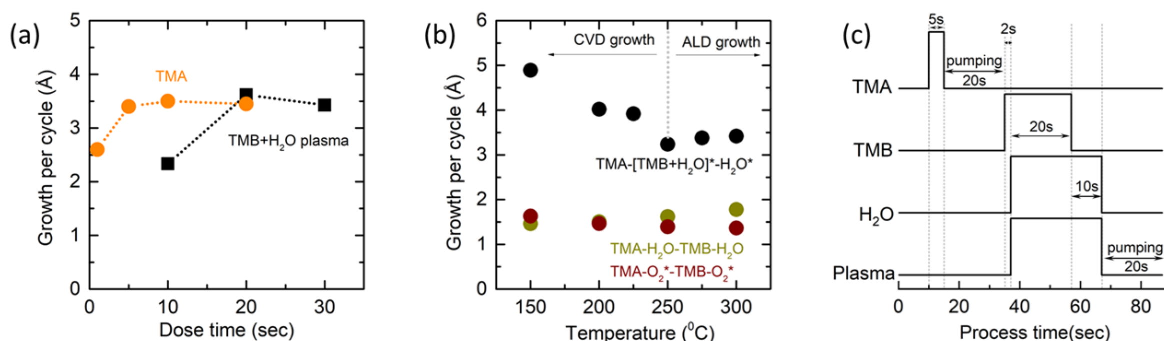

Figure 3: Growth behavior of aluminum borate processes. (a) saturation profile of TMA and (TMB+H_2O) plasma doses for the TMA-[TMB+H_2O]*-H_2O aluminum borate process at 300 °C, (b) growth per cycle of different aluminum borate processes as a function of substrate temperature, and (c) schematic of ALD pulse sequence of aluminum borate films using combined plasma approach.

Figure 3b presents the growth per cycle of aluminum borate films as a function of the substrate temperature. As anticipated from Figure 3a, a stable growth rate was observed at 250 °C and above, while below this temperature, a CVD type growth was observed. A schematic representation of ALD pulse sequence using combined plasma approach is shown in Figure 3c. Growth per cycle values for pure thermal (1.4 Å) and O_2-plasma (1.8 Å) processes are also shown for comparison. More details about these two processes are given in the Supporting Information (Figure S2 and S3).

Table 1 displays the atomic percentages of different elements from various aluminum borate films as determined by ERD analysis. Corresponding ERD survey spectra and depth profiles for these samples are depicted in Figure S4 (supporting data). Films derived from the thermal process exhibit the lowest boron content (~4.1 at%), along with carbon impurities, and the highest H concentration ─ partly originating from unreacted CH_3 species. In the case of the O_2 plasma process, there is an improvement in boron content to ~6.1 at% (almost 50% increase), accompanied by a decrease in C and H concentrations. In the (TMB+H_2O) combined-plasma process, as anticipated, the boron concentration further increases to ~7.7 at%, i.e. more than a 25% increase compared to the O_2 plasma process and more than a 85% increase compared to the thermal process. Interestingly, the (TMB+H_2O) combined-plasma sample also exhibits the lower H concentration among the samples. This could be attributed to the higher substrate temperature in this process. It was observed that films tend to have higher H content at lower deposition temperatures. For instance, films deposited at 100 °C with the four-step O_2 plasma process contain approximately 15 at% H compared to 7 at% H at 150 °C. This is mainly due to the increase in more oxide like surface (-Al-O-Al/B-O-) and decrease in surface hydroxylated surface sites during oxygen plasma step.

Table 1: Elemental compositions as determined by ERD of aluminum borate films obtained from different ALD routes.

ALD process	[Al]	[B]	[O]	[C]	[H]
TMA-H_2O-TMB-H_2O (150 °C)	28.7±1.5	4.1±0.3	53.9±2.4	2.5±0.2	10.7±1.4
TMA-O_2*-TMB-O2* (150 °C)	28±1.5	6.1±0.4	58.9±2.1	0.5±0.1	6.4±0.9

TMA-[TMB+H_2O]*-H_2O* (300 °C)	28.5±1.5	7.7±0.4	58.5±2.1	0.6±0.1	4.8±0.7

UNRAVELLING THE GROWTH MECHANISM DURING ALUMINUM BORATE ALD

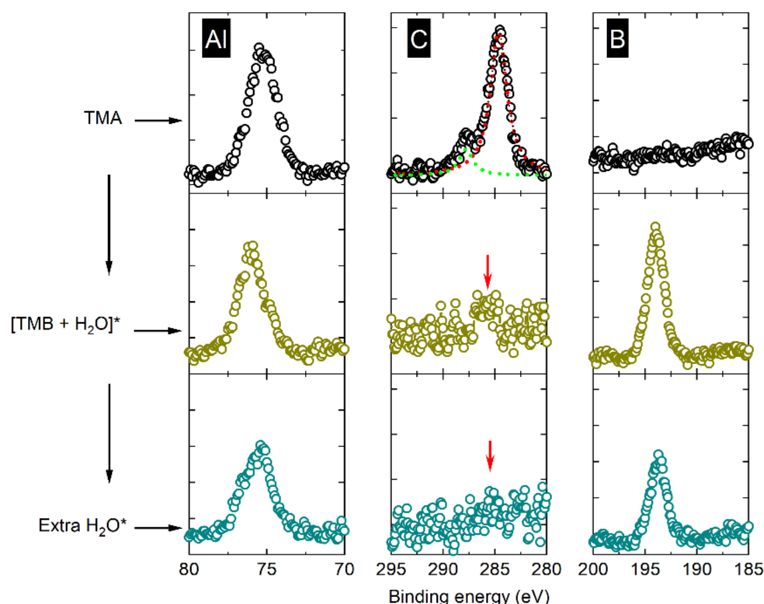

Figure 4: *In vacuo* XPS spectra of Al 2p, C 1s, and B 1s measured after each precursor dose during the (TMB+H_2O) combined-plasma ALD process.

***In vacuo* XPS study.** As explained earlier, *in vacuo* XPS studies were performed in a custom-built cluster tool where an XPS chamber is connected to an ALD chamber and the samples were analyzed after each precursor dosing. To establish a common starting point, the substrate temperature in the ALD chamber was maintained at a constant 300 °C temperature for all the experiments. Prior to dosing any precursor, the SiO_2 substrates underwent a 60 second oxygen plasma pre-clean to remove organic contaminants and achieve a similar initial surface condition. To ensure saturation, each precursor was dosed ten times for 10 seconds, unless specified otherwise.

Figure S5 and S6 present the spectra of Al 2p, C 1s, and B 1s after each precursor dosing for the thermal and O_2 plasma processes respectively. After the TMA dose, a C1s peak at 284.7 eV can be seen in every case which corresponds to Al─CH_3 bonds, and a smaller peak around 288 eV likely corresponds to Si─OCH_3 bonds (Figure S5). Although most of the surface carbon can be removed with the subsequent water pulses, a certain fraction persists even after ten precursor doses. This persistent presence of ─CH_3 has been observed in other studies as well and most likely reacts away in subsequent half-cycles, eventually leaving no carbon incorporated in the film.[38,39] After the TMB dose, two distinct C 1s peaks are observed for the thermal process: one from unreacted Al─CH_3 and another, most likely, from surface ─OCH_3 originating from the TMB molecule. The second H_2O dose following TMB leads to a decrease in the peak intensity of ─OCH_3, but a significant amount of unreacted ligand remains on the surface, which clearly explains why borate films obtained from thermal processes contain a notable amount of carbon. On the other hand, the O_2-plasma steps successfully remove all the surface carbon (Figure S6). It should be noted that the decrease in Al and B peak intensities after the plasma steps may be attributed to the extended plasma exposure time (in total 100 seconds), which results in the etching of some surface species. In a regular ALD process, the optimized plasma exposure time would be much lower, and we expect little or no etching phenomena to occur. Furthermore, the Al/B ratio remains relatively unchanged before and after the plasma step.

In the process with a (TMB+H_2O) combined plasma step, a strong B1s peak was observed as shown in Figure 4, with minimal amount of carbon (~1%) incorporation. Interestingly, as indicated by the arrow, carbon could be further removed by an additional plasma water step, likely due to elimination of unreacted ─OCH_3 species. Therefore, all the growth studies were performed with a 10 second additional water plasma step. This study demonstrates that the combined plasma

approach produces high-quality boron-containing layers with larger boron content than conventional methods. Once again, the reduction in peak intensity is likely due to plasma overexposure, as the Al/B ratio remains unchanged.

In situ mass spectrometry. Traditional QMS measurements observe only a few selected m/z values at high time resolution scales, which may overlook critical mass species. However, acquiring full-range m/z spectra, such as m/z=1-200 amu, requires significant measurement time, making it challenging to measure transient species during an ALD process. To overcome this challenge, our group has reported an innovative way to conduct *in situ* mass spectrometry that provides time-resolved, full-range m/z spectra by exploiting the cyclic nature of the ALD process.[34,35] This approach ensures that no critical mass species are overlooked, providing a comprehensive view of the reaction mechanism. Using this method, we have discovered a previously unknown secondary reaction pathway during the water dose in the TMA─H_2O process.[34] In this work, we utilize this method of mass spectrometry to explore the underlying mechanism of aluminum borate ALD.

Before acquiring the mass spectra data for a full process, it was crucial to first understand the individual background spectra, specifically the TMB plasma and combined plasma. Figure S7 (supporting data) displays all the reference spectra. In the case of TMB plasma, only mass fractions of TMB molecules were observed in the spectra. The absence of any additional peaks up to 200 amu suggests that the polymerized species either have a higher molecular weight or get fragmented into smaller fragments due to ionization. During the combined plasma dose, it is interesting to note that no species corresponding to the TMB molecule could be found. However, the presence of species with m/z=29 (CHO), 31(OCH_3) and 44 (CO_2) confirms the dissociation and *in situ* polymerization of TMB molecules. The absence of any other species in the spectrum indicates the complete dissociation of the available TMB molecules in the plasma.

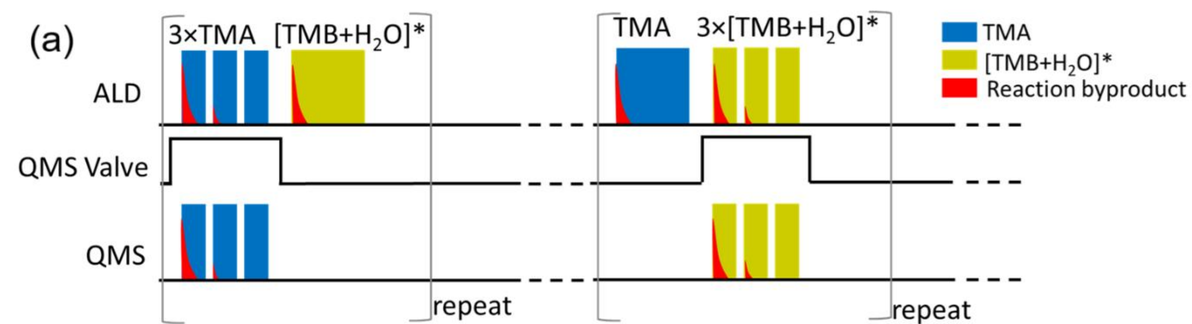

(b)

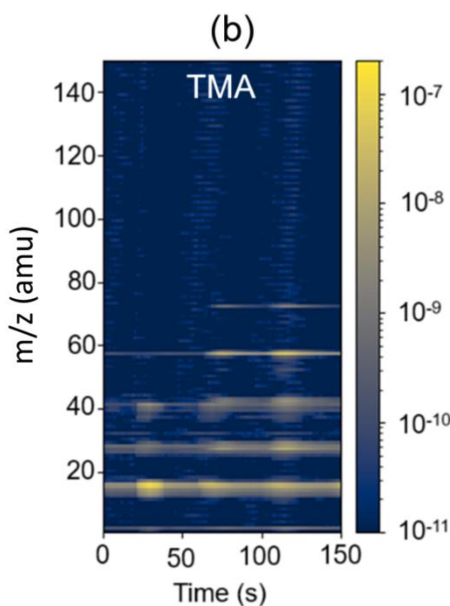

(c)

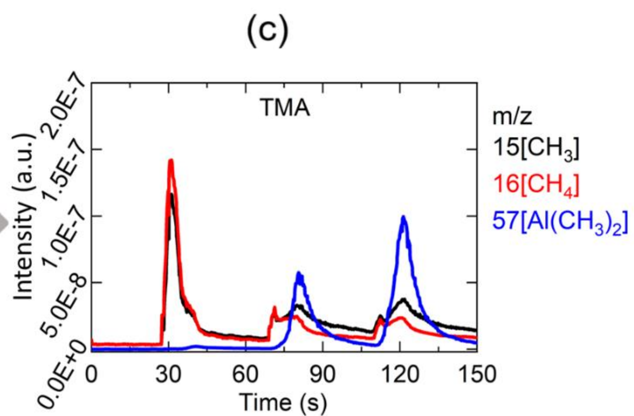

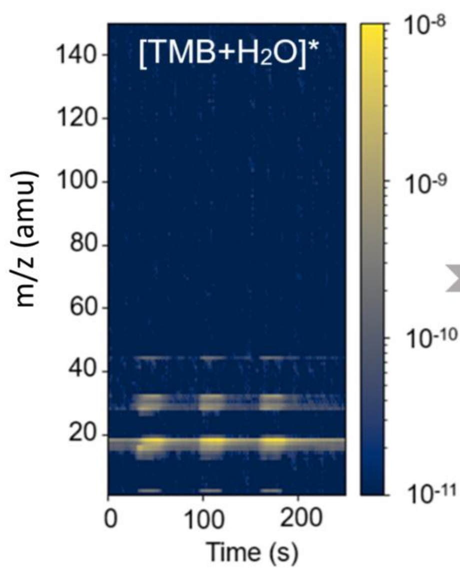

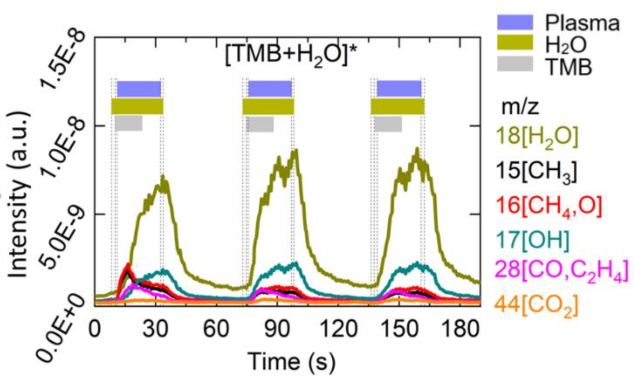

Figure 5: *In situ* transient mass spectra during combined-plasma process. (a) Schematic representation of pulsing and data acquisition sequence for the QMS measurement, (b) individual heat map profiles of atomic mass (m/z) against reaction time during 3xTMA and 3x(TMB+H_2O)-plasma pulses at 300 °C (left), and (c) time-resolved mass spectra of few selected mass species extracted from the heat map to understand the transient nature of by-products (right).

Figure 5a illustrates the process sequence for acquiring mass spectroscopy data and Figure 5b represents the time-resolved heat map profile with m/z values (1-150 amu) during 3xTMA and 3x(TMB+H_2O)-plasma doses. Transient data of a few selected byproducts with corresponding m/z values extracted from the heat map profiles are presented in Figure 5b. It is noteworthy that the individual heat map profile data were accumulated over 30 ALD cycles. Data acquisition and analysis details is explained in our previous articles.[34,35] During the first TMA pulse, the lack of m/z peaks at 57 and 72, corresponding to $Al(CH_3)_2$ and $Al(CH_3)_3$ fragments, respectively, indicate that the majority of the precursor is consumed by the surface species in the first pulse. In the subsequent doses, only a small fraction of the precursor interacts, while the majority remains unreacted, indicating self-saturating behavior in the ALD reaction. The time-resolved profile shown in Figure 5c of m/z=15 (CH_3) and 16 (CH_4) provides a closer look at the main byproduct, CH_4. It is evident that most of the byproducts are observed during the initial few seconds of the first TMA pulse. In the subsequent TMA pulses, only a small amount of CH_4 evolved initially, and most of the CH_4 and CH_3 signal arises from unreacted TMA molecules later.

The spectrum during (TMB+H_2O) combined plasma step is particularly interesting, primarily due to the transient nature of a few species. Firstly, it is evident that the maximum amount of water (m/z=18) consumption, and hence the maximum release of byproducts, occurs during the first few

seconds of the first dose. The masses corresponding to the CH_3 and CH_4 (m/z= 15 and 16) species exhibit a peak intensity during the initial seconds and then gradually reach saturation. No transient behavior is observed from the second dose onwards. The same trend applies to the signal at 28 corresponding to the CO species, which is likely obtained due to the oxidation of CH_3 species. Even after closing the TMB valve, significant signals at m/z= 28 and 44 are observed. In conjunction with the *in vacuo* XPS results, this phenomenon can be explained by the fact that the water plasma continues to oxidize any remaining surface carbon species on substrate and reactor walls. Similar measurements were also conducted and presented in Figure S8 and S9 (supporting info) for thermal and O_2 plasma processes, respectively. The thermal process shows slow and lower interaction between surface ─B-OCH_3 and incoming H_2O molecules whereas plasma processes are quite fast and saturation obtained within a few seconds of exposure.

DISCUSSION

Plasma polymerization in ALD processes can be advantageous for growing challenging materials, but achieving self-limiting growth requires reaching a ceiling point. The ceiling point is the temperature or condition where the polymerization process halts due to thermodynamic limitations. At this point, the rates of polymerization and depolymerization are balanced, preventing further polymer growth, often due to thermal degradation or deactivation under certain conditions.

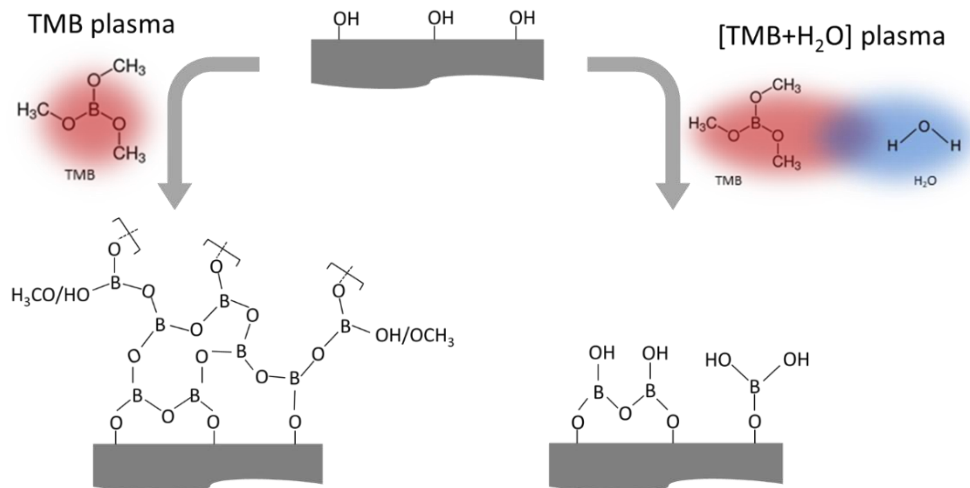

Figure 6: Schematic illustration of proposed reaction pathways during TMB and [TMB+H_2O] plasma steps.

In our study, the ceiling point of TMB plasma alone was not achieved within a suitable temperature range, making it unsuitable as precursor for an ALD process. However, the introduction of water into TMB plasma with optimized partial pressure enabled the achievement of a ceiling point, allowing it to be used effectively in an ALD process. The ceiling point likely corresponds to the saturation of the hydroxylation reaction, where the formation of hydroxyl groups on the surface halts further growth, limiting it to a (mono)layer of boron-containing layer with hydroxyl-type surface termination. Without the presence of sufficient OH radicals, surface saturation does not occur, making polymerization growth more favorable. Figure 6 illustrates a schematic representation of the plasma polymerization process with and without the presence of water in the plasma.

As observed from OES and QMS spectra, TMB plasma generates most of the radicals or ions that are also found in O_2 or H_2O plasma. Although OH emission is detected in TMB plasma, its intensity is relatively low compared to other species. When O_2 is introduced into the TMB plasma (TMB + O_2), the OH peak intensity increases slightly, likely due to the *in situ* combination of O

and H species. However, the most significant difference is observed in the TMB + H_2O plasma, where OH emission is considerably stronger. This indicates that the high concentration of OH radicals play a crucial role in achieving self-limiting growth, while the presence of additional species like O and H further enhances the process. A list of probable plasma generated species from different vapors is presented in Table S1 (supporting info).

This hypothesis is further supported by *in vacuo* XPS analysis. We performed deconvolution of the O 1s and B 1s peaks for both TMB plasma and TMB + H_2O plasma processes (presented in Figure S10 in supporting info). For TMB plasma, the composition of B–O and B–OH species was found to be 76% and 24%, respectively. In contrast, for the TMB + H_2O plasma process, these percentages shifted to 68% and 32%. The O 1s peaks are more complex due to the presence of multiple bonding environments, but from our deconvolution and fitting analysis, the B–OH to B–O ratio increased from 0.45 (TMB plasma) to 0.7 (TMB + H_2O plasma). These findings strongly indicate that the OH species generated during the plasma step play a crucial role in achieving self-limiting growth.

CONCLUSIONS

Our findings reveal that a hybrid plasma approach not only enhances the growth per cycle but also improves boron concentration in aluminum borate films, opening new avenues for developing boron-containing layers via the ALD method. In-depth studies using OES, *in vacuo* XPS and *in situ* mass spectrometry provide valuable insights into reaction pathways and difficulties involved with different ALD routes to produce metal borate layers. For thermal processes, the slow reaction between TMB and water results in incomplete reactions, whereas the O_2 plasma process results in partial consumption of surface ─O(H) species by ─$O(CH_3)$ ligands. The absence of a ceiling point makes TMB plasma alone unsuitable for ALD. However, the presence of hydroxyl species during the combined plasma pulse along with optimized partial pressures and substrate temperature creates favorable conditions for self-limiting growth of boron-containing layers. The concept illustrated here for Aluminum borate can potentially be generalized towards ALD of other metal borates as well, thus offering promising opportunities for the deposition of boron-containing nanocoatings with improved properties.

ACKNOWLEDGMENTS

This work was financially supported by the UGENT-GOA-01G02124 project and Fonds Wetenschappelijk Onderzoek – Vlaanderen (FWO) by providing Tippi Verhelle with an SB grant (1SH9024N) and Lowie Henderick with a junior postdoctoral fellowship (1254324N).

SUPPORTING INFORMATION DESCRIPTION

Growth study of BO_x with *in situ* ellipsometry; *In situ* ellipsometry data of different thermal processes; *In situ* ellipsometry data of different oxygen plasma processes; ERD survey spectra and corresponding depth profiles of different aluminum borate films; *In vacuo* XPS spectra for the

TMA-H_2O-TMB-H_2O thermal process; *In vacuo* XPS spectra for the TMA-O_2*-TMB-O_2* process; Plasma generated species; QMS reference mass spectra of different reactants; QMS data acquisition scheme and obtained data of the TMA-H_2O-TMB-H_2O thermal process; QMS data acquisition scheme and obtained data of the TMA-O_2*-TMB-O_2* process; *In vacuo* XPS analysis; SEM and AFM of different plasma approaches

REFERENCES

(1) Kim, W.-H.; Oh, I.-K.; Kim, M.-K.; Maeng, W. J.; Lee, C.-W.; Lee, G.; Lansalot-Matras, C.; Noh, W.; Thompson, D.; Chu, D.; Kim, H. Atomic Layer Deposition of B_2O_3/SiO_2 Thin Films and Their Application in an Efficient Diffusion Doping Process. *J. Mater. Chem. C* **2014**, *2*, 5805.

(2) Kalkofen, B.; Amusan, A. A.; Bukhari, M. S. K.; Garke, B.; Lisker, M.; Gargouri, H.; Burte, E. P. Use of B_2O_3 Films Grown by Plasma-Assisted Atomic Layer Deposition for Shallow Boron Doping in Silicon. *J. Vac. Sci. Technol. A* **2015**, *33*, 031512.

(3) Appleby, G. A.; Vontobel, P. Optimisation of Lithium Borate–Barium Chloride Glass-Ceramic Thermal Neutron Imaging Plates. *Nucl. Instrum. Methods Phys. Res. A* **2008**, *594*, 253–256.

(4) Wang, Z.; Morris, C. L. Multi-Layer Boron Thin-Film Detectors for Neutrons. *Nucl. Instrum. Methods Phys. Res. A* **2011**, *652*, 323–325.

(5) Meng, Y.; Ni, G.; Jin, X.; Peng, J.; Yan, Q. Y. Recent Advances in the Application of Phosphates and Borates as Electrocatalysts for Water Oxidation. *Mater. Today Nano* **2020**, *12*, 100095.

(6) You, C.; Ji, Y.; Liu, Z.; Xiong, X.; Sun, X. Ultrathin CoFe-Borate Layer Coated CoFe-Layered Double Hydroxide Nanosheets Array: A Non-Noble-Metal 3D Catalyst Electrode for Efficient and Durable Water Oxidation in Potassium Borate. *ACS Sustainable Chem. Eng.* **2018**, *6*, 1527–1531.

(7) Barpanda, P.; Dwibedi, D.; Ghosh, S.; Kee, Y.; Okada, S. Lithium Metal Borate ($LiMBO_3$) Family of Insertion Materials for Li-Ion Batteries: A Sneak Peak. *Ionics* **2015**, *21*, 1801–1812.

(8) Yang, S.-H.; Xue, H.; Guo, S.-P. Borates as Promising Electrode Materials for Rechargeable Batteries. *Coord. Chem. Rev.* **2021**, *427*, 213551.

(9) Lepry, W. C.; Nazhat, S. N. A Review of Phosphate and Borate Sol–Gel Glasses for Biomedical Applications. *Adv. NanoBiomed Res.* **2021**, *1*, 2000055.

(10) Kobayashi, K. Applications of BN- and ZnF_2-Containing Zinc Borate Glasses to Laser-Annealed Polycrystalline Si Field Effect Transistors. *Mater. Res. Bull.* **1998**, *33*, 1257–1263.

(11) Hu, W.; Zhang, C.; Jiang, H.; Zheng, M.; Wu, Q.-H.; Dong, Q. Improving the Electrochemistry Performance of Layer $LiNi_{0.5}Mn_{0.3}Co_{0.2}O_2$ Material at 4.5V Cutoff Potential Using Lithium Metaborate. *Electrochim. Acta* **2017**, *243*, 105–111.

(12) Lee, S. H.; Cho, K. I.; Shin, D. W. Conductivity of Lithium Borophosphate Glasses for Thin Film Solid Electrolyte of Lithium Battery. *ECS Meeting Abstracts* **2006**, *MA2006-01*, 159.

(13) Fleutot, B.; Pecquenard, B.; Martinez, H.; Levasseur, A. Lithium Borophosphate Thin Film Electrolyte as an Alternative to LiPON for Solder-Reflow Processed Lithium-Ion Microbatteries. *Solid State Ion.* **2013**, *249–250*, 49–55.

(14) Kazyak, E.; Chen, K.-H.; Davis, A. L.; Yu, S.; Sanchez, A. J.; Lasso, J.; Bielinski, A. R.; Thompson, T.; Sakamoto, J.; Siegel, D. J.; Dasgupta, N. P. Atomic Layer Deposition and First Principles Modeling of Glassy Li_3BO_3–Li_2CO_3 Electrolytes for Solid-State Li Metal Batteries. *J. Mater. Chem. A* **2018**, *6*, 19425–19437.

(15) Kazyak, E.; Chen, K.-H. (Michael); Chen, Y.; Dasgupta, N. P. Inhibiting Li Plating on Graphite Electrodes during 4C Fast-Charging with Atomic Layer Deposition. *ECS Meeting Abstracts* **2021**, *MA2021-02*, 459.

(16) Zhang, X.; Wang, B.; Huang, W.; Chen, Y.; Wang, G.; Zeng, L.; Zhu, W.; Bedzyk, M. J.; Zhang, W.; Medvedeva, J. E.; Facchetti, A.; Marks, T. J. Synergistic Boron Doping of Semiconductor and Dielectric Layers for High-Performance Metal Oxide Transistors: Interplay of Experiment and Theory. *J. Am. Chem. Soc.* **2018**, *140*, 12501–12510.

(17) George, S. M. Atomic Layer Deposition: An Overview. *Chem. Rev.* **2010**, *110*, 111–131.

(18) Mackus, A. J. M.; Schneider, J. R.; MacIsaac, C.; Baker, J. G.; Bent, S. F. Synthesis of Doped, Ternary, and Quaternary Materials by Atomic Layer Deposition: A Review. *Chem. Mater.* **2019**, *31*, 1142–1183.

(19) Mattelaer, F.; Van Daele, M.; Minjauw, M. M.; Nisula, M.; Elliott, S. D.; Sajavaara, T.; Dendooven, J.; Detavernier, C. Atomic Layer Deposition of Localized Boron- and Hydrogen-Doped Aluminum Oxide Using Trimethyl Borate as a Dopant Precursor. *Chem. Mater.* **2020**, *32*, 4152–4165.

(20) Saly, M. J.; Munnik, F.; Baird, R. J.; Winter, C. H. Atomic Layer Deposition Growth of BaB2O4 Thin Films from an Exceptionally Thermally Stable Tris(Pyrazolyl)Borate-Based Precursor. *Chem. Mater.* **2009**, *21*, 3742–3744.

(21) Saly, M. J.; Munnik, F.; Winter, C. H. Atomic Layer Deposition of CaB_2O_4 Films Using Bis(Tris(Pyrazolyl)Borate)Calcium as a Highly Thermally Stable Boron and Calcium Source. *J. Mater. Chem.* **2010**, *20*, 9995–10000.

(22) Sevim, F.; Demir, F.; Bilen, M.; Okur, H. Kinetic Analysis of Thermal Decomposition of Boric Acid from Thermogravimetric Data. *Korean J. Chem. Eng.* **2006**, *23*, 736–740.

(23) Pankajavalli, R.; Anthonysamy, S.; Ananthasivan, K.; Vasudeva Rao, P. R. Vapour Pressure and Standard Enthalpy of Sublimation of H_3BO_3. *J. Nucl. Mater.* **2007**, *362*, 128–131.

(24) Mane, A. U.; Elam, J. W. Method of Creating Boron Comprising Layer, US patent no. 10294564B2, May 2019.

(25) Dobbelaere, T.; Roy, A. K.; Vereecken, P.; Detavernier, C. Atomic Layer Deposition of Aluminum Phosphate Based on the Plasma Polymerization of Trimethyl Phosphate. *Chem. Mater.* **2014**, *26*, 6863–6871.

(26) Dobbelaere, T.; Mattelaer, F.; Dendooven, J.; Vereecken, P.; Detavernier, C. Plasma-Enhanced Atomic Layer Deposition of Iron Phosphate as a Positive Electrode for 3D Lithium-Ion Microbatteries. *Chem. Mater.* **2016**, *28*, 3435–3445.

(27) Dobbelaere, T.; Mattelaer, F.; Roy, A. K.; Vereecken, P.; Detavernier, C. Plasma-Enhanced Atomic Layer Deposition of Titanium Phosphate as an Electrode for Lithium-Ion Batteries. *J. Mater. Chem. A* **2017**, *5*, 330–338.

(28) Dobbelaere, T.; Mattelaer, F.; Vereecken, P. M.; Detavernier, C. Plasma-Enhanced Atomic Layer Deposition of Vanadium Phosphate as a Lithium-Ion Battery Electrode Material. *J. Vac. Sci. Technol. A* **2017**, *35*, 041513.

(29) Dobbelaere, T.; Minjauw, M.; Ahmad, T.; Vereecken, P. M.; Detavernier, C. Plasma-Enhanced Atomic Layer Deposition of Zinc Phosphate. *J. Non-Cryst. Solids* **2016**, *444*, 43–48.

(30) Henderick, L.; Blomme, R.; Minjauw, M.; Keukelier, J.; Meersschaut, J.; Dendooven, J.; Vereecken, P.; Detavernier, C. Plasma-Enhanced Atomic Layer Deposition of Nickel and Cobalt Phosphate for Lithium Ion Batteries. *Dalton Trans.* **2022**, *51*, 2059–2067.

(31) Belousov, M. E.; Mankelevich, Y. A.; Minakov, P. V.; Rakhimov, A. T.; Suetin, N. V.; Khmelnitskiy, R. A.; Tal, A. A.; Khomich, A. V. Boron-Doped Homoepitaxial Diamond CVD from Microwave Plasma-Activated Ethanol/Trimethyl Borate/Hydrogen Mixtures. *Chem. Vap. Depos.* **2012**, *18*, 302–308.

(32) Marton, M.; Vojs, M.; Michniak, P.; Behúl, M.; Rehacek, V.; Pifko, M.; Stehlík, Š.; Kromka, A. New Chemical Pathway for Large-Area Deposition of Doped Diamond Films by Linear Antenna Microwave Plasma Chemical Vapor Deposition. *Diam. Relat. Mater.* **2022**, *126*, 109111.

(33) Fairley, N.; Fernandez, V.; Richard-Plouet, M.; Guillot-Deudon, C.; Walton, J.; Smith, E.; Flahaut, D.; Greiner, M.; Biesinger, M.; Tougaard, S.; Morgan, D.; Baltrusaitis, J. Systematic and Collaborative Approach to Problem Solving Using X-Ray Photoelectron Spectroscopy. *Appl. Surf. Sci. Adv.* **2021**, *5*, 100112.

(34) Werbrouck, A.; Shirazi, M.; Mattelaer, F.; Elliott, S. D.; Dendooven, J.; Detavernier, C. A Secondary Reaction Pathway for the Alumina Atomic Layer Deposition Process with Trimethylaluminum and Water, Revealed by Full-Range, Time-Resolved In Situ Mass Spectrometry. *J. Phys. Chem. C* **2020**, *124*, 26443–26454.

(35) Werbrouck, A.; Mattelaer, F.; Minjauw, M.; Nisula, M.; Julin, J.; Munnik, F.; Dendooven, J.; Detavernier, C. Reaction Pathways for Atomic Layer Deposition with Lithium Hexamethyl Disilazide, Trimethyl Phosphate, and Oxygen Plasma. *J. Phys. Chem. C* **2020**, *124*, 27829–27839.

(36) Friedrich, J. Mechanisms of Plasma Polymerization – Reviewed from a Chemical Point of View. *Plasma Process. Polym.* **2011**, *8*, 783–802.

(37) Henderick, L.; Dhara, A.; Werbrouck, A.; Dendooven, J.; Detavernier, C. Atomic Layer Deposition of Metal Phosphates. *Appl. Phys. Rev.* **2022**, *9*, 011310.

(38) Vandalon, V.; Kessels, W. M. M. (Erwin). Revisiting the Growth Mechanism of Atomic Layer Deposition of Al_2O_3: A Vibrational Sum-Frequency Generation Study. *J. Vac. Sci. Technol. A* **2017**, *35*, 05C313.

(39) Nieminen, H.-E.; Chundak, M.; Heikkilä, M. J.; Kärkkäinen, P. R.; Vehkamäki, M.; Putkonen, M.; Ritala, M. In Vacuo Cluster Tool for Studying Reaction Mechanisms in Atomic Layer Deposition and Atomic Layer Etching Processes. *J. Vac. Sci. Technol. A* **2023**, *41*, 022401.

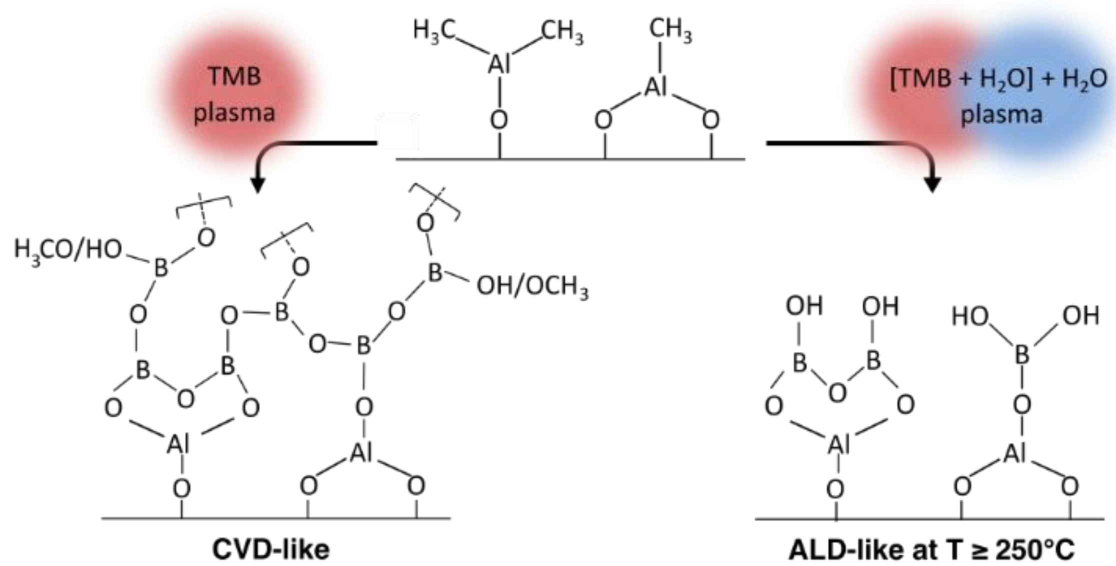

Figure 7: ToC graphic